Active control and switching of broadband electromagnetically induced transparency in symmetric metadevices

Yahiaoui, Riad; Manjappa, Manukumara; Srivastava, Yogesh Kumar; Singh, Ranjan

2017

Yahiaoui, R., Manjappa, M., Srivastava, Y. K., & Singh, R. (2017). Active control and switching of broadband electromagnetically induced transparency in symmetric metadevices. Applied Physics Letters, 111(2), 021101-.

https://hdl.handle.net/10356/82307

https://doi.org/10.1063/1.4993428

Active control and switching of broadband electromagnetically induced transparency in symmetric metadevices

Riad Yahiaoui,[1,a)] Manukumara Manjappa,[2,3] Yogesh Kumar Srivastava,[2,3] and Ranjan Singh[2,3,a)]
[1]*LEME, EA 4416, Université Paris Nanterre, 50 Rue de Sèvres, 92410 Ville d'Avray, France*
[2]*Division of Physics and Applied Physics, School of Physical and Mathematical Sciences, Nanyang Technological University, 21 Nanyang Link, Singapore 637371, Singapore*
[3]*Center for Disruptive Photonic Technologies, The Photonics Institute, Nanyang Technological University, 50 Nanyang Avenue, Singapore 639798, Singapore*

(Received 11 May 2017; accepted 27 June 2017; published online 10 July 2017)

Electromagnetically induced transparency (EIT) arises from coupling between the bright and dark mode resonances that typically involve subwavelength structures with broken symmetry, which results in an extremely sharp transparency band. Here, we demonstrate a tunable broadband EIT effect in a symmetry preserved metamaterial structure at the terahertz frequencies. Alongside, we also envisage a photo-active EIT effect in a hybrid metal-semiconductor metamaterial, where the transparency window can be dynamically switched by shining near-infrared light beam. A robust coupled oscillator model explains the coupling mechanism in the proposed design, which shows a good agreement with the observed results on tunable broadband transparency effect. Such active, switchable, and broadband metadevices could have applications in delay bandwidth management, terahertz filtering, and slow light effects. *Published by AIP Publishing.*
[http://dx.doi.org/10.1063/1.4993428]

In recent years, the classical analogue of the electromagnetically induced transparency (EIT) phenomenon mimicking the quantum interference effects has attracted much interest due to its numerous potential applications, including plasmonic sensing,[1,2] dynamic storage of light,[3] slow light devices,[4,5] and reduction of losses.[6] Fundamentally, EIT arises from destructive quantum interference between two different excitation pathways in a three level atomic system, making an initially opaque medium transparent to a resonant probe laser beam.[7,8] Practical applications of EIT in atomic systems, however, are severely limited by the necessity for the cryogenic temperature environment and high intensity lasers. Thanks to the advent of metamaterials and motivated by the perspectives of achieving new potential applications,[9–18] a wide variety of metamaterial structures with the advantage of a room-temperature operation have been proposed to mimic the original quantum phenomenon of EIT or the plasmonic analogue of electromagnetically induced transparency.[19–29]

In classical systems, such as metamaterials, the coupling of a bright and a dark resonance can lead to destructive interference between the near fields of the neighboring resonators, thus giving rise to a classical analog of EIT exhibiting a narrow transparency window within a broad absorption band. Due to the resonant nature of metamaterials, the EIT effect based on metamaterials is achieved only in a very narrow frequency range, which may limit its practical applications. Some efforts have been made in demonstrating a broadband EIT effect in the terahertz regime[25] and reported a possible achievement of a broadband slow light optical metamaterial using a multilayer approach.[26] Seeking new designs to achieve a transparency window over a broad spectral range is still in progress and remains a challenge. In most of the previously reported works, it was considered that the asymmetry of the unit cell is a prerequisite for the manifestation of the EIT effect,[27–29] and relatively few works have proposed schemes and designs for the generation of such a phenomenon in symmetric structures.[30–32] In the absence of asymmetry, only a single resonance dip appears in the transmission spectrum without any sign of the EIT effect, which is due to the absence of coupling between the bright and the dark resonance modes. However, here, we propose a novel design of an extremely simple and symmetrical metamaterial structure that shows a tunable broadband EIT effect in the terahertz (THz) frequency regime. The concept of an actively controlled EIT metamaterial enabling the transition from an EIT mode to a dipole mode is also demonstrated numerically and experimentally by modulating the intensity of the external pump laser beam applied to the structure.

The metallic cross-shaped resonators (CSRs) for the passive samples were made from 200 nm thick aluminum (Al) patterned on a 500 μm thick silicon substrate using a photolithography-based patterning process, as shown in Figs. 1(a) and 1(b). The relevant geometrical dimensions of the elementary cell of the CSR metamaterial are as follows: $l = 120\,\mu$m, $w = 20\,\mu$m, $p_x = p_y = 150\,\mu$m, and $d_x = 25$, 30, 40, and 60 μm. Numerical calculations were carried out using the commercial finite difference time domain (FDTD) software package (CST Microwave Studio). In these calculations, the elementary cell of the designed metamaterial was irradiated at normal incidence with the electric field parallel to the x-axis and the magnetic field parallel to the y-axis. Periodic boundary conditions were applied in the numerical model in order to mimic the functioning of a 2D infinite

[a)]Authors to whom correspondence should be addressed: riad.yahiaoui@parisnanterre.fr and ranjans@ntu.edu.sg

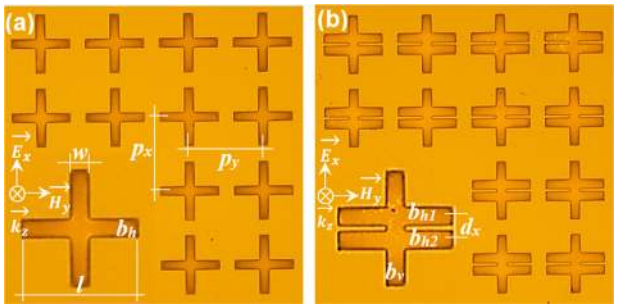

FIG. 1. (a) Optical micrograph of the fabricated CSRs with the corresponding electromagnetic excitation configuration. (b) Optical micrograph of the fabricated EIT metamaterial with the corresponding electromagnetic excitation configuration. The relevant geometrical dimensions are as follows: $p_x = p_y = 150\ \mu$m, $l = 120\ \mu$m, $w = 20\ \mu$m, and $d_x = 25$, 30, 40, and 60 μm.

structure. In simulation, silicon (Si) was treated as a lossless dielectric with $\varepsilon_{Si} = 11.7$ and the aluminum (Al) was modeled as a lossy metal with a conductivity of 3.45×10^7 S/m. The surface area of the fabricated device is about 1 cm × 1 cm, and measurements were performed using the ZnTe crystal based terahertz time domain spectroscopy system in a dry-N_2 environment to prevent undesirable atmospheric absorption. The transmission response of the sample ($E_S(\omega)$) is normalized to the transmission through the reference substrate ($E_R(\omega)$) using the relation $|T(\omega)| = |\frac{E_s(\omega)}{E_R(\omega)}|$.[33,34]

The simulated (solid blue line) and measured (short-dashed green line) transmission spectra of the metamaterial slab are plotted in Fig. 2 and are in good agreement with each other. For the chosen symmetric geometry, the resonance frequency of the resulting dipolar mode [shown in Fig. 2(a)] is around 0.46 THz, with a quality factor of $Q \approx 2.78$, estimated from the linewidth of the resonance dip [the Q factor is obtained from the transmission curve, $Q = \omega_0/\Delta\omega$, where ω_0 is the resonance frequency and $\Delta\omega$ is the full width at half maximum (FWHM) bandwidth]. By splitting the horizontal bar b_h (i.e., the one that is oriented perpendicularly to the electric field $\boldsymbol{E}_x$) of the CSRs into two new bars b_{h1} and b_{h2} separated by a distance $d_x = 25\ \mu$m [see Fig. 1(b)], a typical EIT spectral response is observed, as shown in Fig. 3(a), where a transmission peak appears at about 0.47 THz with an amplitude of 0.75 between two resonance dips at around 0.38 THz and 0.57 THz, respectively. The underlying mechanism of the EIT effect can be understood as the Fano type of interference between the *super-radiant dipole* mode and the *sub-radiant LC* mode of the SRR in the proposed design.

Under the illumination of a linearly polarized THz wave ($\boldsymbol{E}_x$), each unit cell of the EIT metamaterial can be assimilated to a plasmonic "molecule" consisting of a vertical bar (b_v) supporting the dipole type resonance, and the split bars (b_{h1} and b_{h2}) together with a part of b_v form a SRR structure, thus supporting LC type of resonance [shown in Figs. 2(a) and 2(b), respectively]. Despite the fact that both the resonators are directly excited by the incoming terahertz wave, the dipole resonance possessing the lower Q-factor ($Q = 2.78$) serves as the "bright" mode and the LC resonance displaying higher Q-factor ($Q = 15.6$) acts as the sub-radiant "quasi-dark" mode in the system. In such type of systems, the necessary condition to achieve EIT is to couple the bright and quasi-dark resonances possessing contrasting line widths and resonating at the same resonance frequency.[22–24,32] Hence, the coupling between the vertical bar (b_v) and the split bars (b_{h1} and b_{h2}) leads to a narrow transmission peak at the center of the broad transmission dip [see Fig. 3(a)], thus confirming the Fano-type of destructive interference between the near fields of the two classical resonators. A much broader band of transparency window can be achieved by gradually increasing the displacement d_x between the bars b_{h1} and b_{h2}. As shown in Figs. 3(a)–3(d), upon increasing d_x, the spectral width of the EIT window significantly increases with a noticeable enhancement in its amplitude. For instance, the full width at half maximum (FWHM) bandwidth of the transparency window for the simulated (shown in blue) curve extends from 0.42 THz at $d_x = 25\ \mu$m to 0.56 THz at $d_x = 30\ \mu$m, whereas for larger separation d_x, this range is much broader, namely, for $d_x = 60\ \mu$m, the FWHM bandwidth of the transparency region spans over 360 GHz, corresponding to nearly 65.45% of the central frequency value.

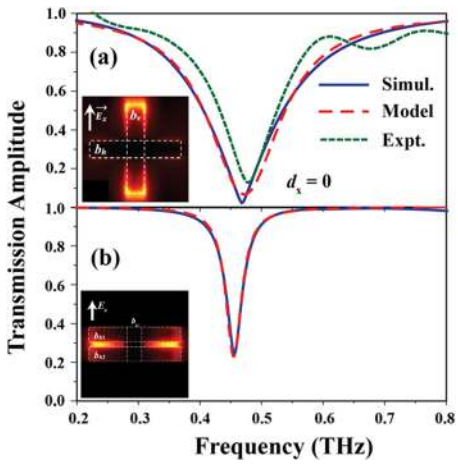

FIG. 2. (a) and (b) Simulated (solid blue line) and measured (short dashed green line) terahertz transmission spectra of the CSRs ($d_x = 0\ \mu$m) and SRR, respectively. The red dashed curves represent the analytically fitted data ($T = 1\text{-Im}(\chi)$) using the two-oscillator model [Eq. (3)]. The inset diagram in (a) and (b) represents the electric field distribution in the symmetric dipole structure and the horizontal bars with a part of vertical bar forming the SRR resonators, respectively.

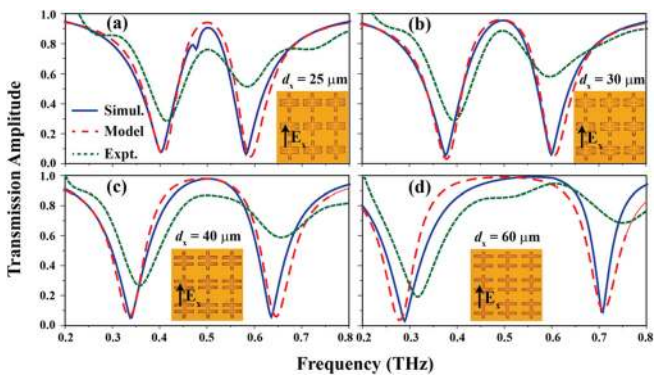

FIG. 3. (a)–(d) Simulated (solid blue line) and measured (short dashed green line) terahertz transmission spectra of the EIT metamaterial for increased separation $d_x = 25\ \mu$m, 30 μm, 40 μm, and 60 μm between the horizontal bars, respectively. The red dashed curves represent the analytically fitted data ($T = 1\text{-Im}(\chi)$) using the two-oscillator model [Eq. (3)]. The inset pictures illustrate the optical microscopy images of the fabricated passive samples with varying d_x.

Recently, a broad transparency window across a frequency range greater than 0.61 THz in the transmittance spectrum has been reported numerically.[33]

To demonstrate the validity of the underlying EIT metamaterial, we used the analytical model based on the coupled oscillator theory described by the following set of equations:[23]

$$\ddot{x}_b(t) + \gamma_b \dot{x}_b(t) + {\omega_b}^2 x_b(t) + \Omega^2 x_d(t) = f_b E, \quad (1)$$

$$\ddot{x}_d(t) + \gamma_d \dot{x}_d(t) + {\omega_d}^2 x_d(t) + \Omega^2 x_b(t) = f_d E. \quad (2)$$

Here, ω_b, ω_d and γ_b, γ_d are the resonance angular frequencies and the loss-factors of the bright and quasi-dark particles, respectively. Ω defines the coupling strength between the bright and quasi-dark particles. $f_b = Q/M$ and $f_d = q_d/m_d$ are the free space coupling strengths of bright and the quasi-dark modes with the incident THz light, where (Q, q_d) and (M, m_d) are their effective charge and mass, respectively. The transmission curves in Figs. 2 and 3 are fitted by the imaginary part of nonlinear susceptibility expression (χ) obtained by solving the coupled equations (1) and (2) for x_b and x_d, which is given by

$$\chi = \frac{{q_d}^2 mK}{Q^2 M}\left(\frac{\frac{Q}{q_d}\left(\frac{M}{m_d}+1\right)\Omega^2 + \left(\frac{Q}{q_d}\right)^2\left((\omega^2-{\omega_d}^2)+\left(\frac{M}{m_d}\right)(\omega^2-{\omega_b}^2)\right)}{\Omega^4 - (\omega^2-{\omega_b}^2+i\omega\gamma_b)(\omega^2-{\omega_d}^2+i\omega\gamma_d)} + i\omega\frac{\left(\frac{Q}{q_d}\right)^2\gamma_d + \frac{M}{m_d}\gamma_b}{\Omega^4 - (\omega^2-{\omega_b}^2+i\omega\gamma_b)(\omega^2-{\omega_d}^2+i\omega\gamma_d)}\right). \quad (3)$$

Analytically modeled transmission data are represented by the red dashed curves in Figs. 2 and 3, which show good agreement with the corresponding numerically simulated curves plotted for the EIT system with varying d_x. In our fitting, the transmission coefficient is defined as $T = 1\text{-Im}(\chi)$ (given by the Kramer-Kronig relations), which is derived from the conservation of energy relation $T + A = 1$ (normalized to unity), where $A = \text{Im}(\chi)$ is the absorption/losses in the medium. We neglect other nonresonant scattering losses, which are negligible in the system and do not show any effect on the experimentally observed/simulated resonance characteristics. As the condition for EIT demands, in the analytical model, the resonance frequencies of the bright and the quasi-dark modes are kept constant (ω_b, $\omega_d = 3.2 \times 10^{12}$ rad/s), whereas their line widths differ by an order of magnitude ($\gamma_d = 0.1\gamma_b$). The tuning of the transparency bandwidth by changing d_x is dictated by the corresponding coupling strength (Ω) between the bright and the quasi-dark mode and their direct individual coupling with the free space light, which is quantified by the values of f_b and f_d. A good agreement between the analytical data and the corresponding simulations is achieved for the coupling parameters $\Omega = 1.9 \times 10^{12}$, 2.2×10^{12}, 2.45×10^{12}, and 2.7×10^{12} rad/s for $d_x = 25$, 30, 40, and 60 μm, respectively. Similarly, using the proposed model, we quantify the relative coupling of the bright and the quasi-dark mode to the free space field using the ratio f_b/f_d, where for $d_x = 25$, 30, 40, and 60 μm, the free space coupling ratios are $f_b/f_d = 10$, 9, 6, and 4.5, respectively. The decreasing f_b/f_d signifies that, as the separation between the horizontal bars (d_x) is increased, the quasi-dark mode (SRR resonator) starts to couple strongly to the incident THz field and hence is responsible for the increased line width of the transparency window (which is mainly dictated by the discreteness of the dark state resonance). In Figs. 4(a)–4(d), we show the electric field distribution calculated at the transparency peak (0.5 THz) for varying "d_x," wherein the fields confined between the horizontal bars signify the presence of the SRR effect that serves as the quasi-dark mode in the proposed EIT structure. As the separation "d_x" between the horizontal bars is increased from 25 μm to 60 μm, the confinement of the electric fields in the SRR gap gradually decreases, indicating the increased radiative nature of the SRR (quasi-dark) structures, which is a direct consequence of the increased coupling of SRR to the free space field.

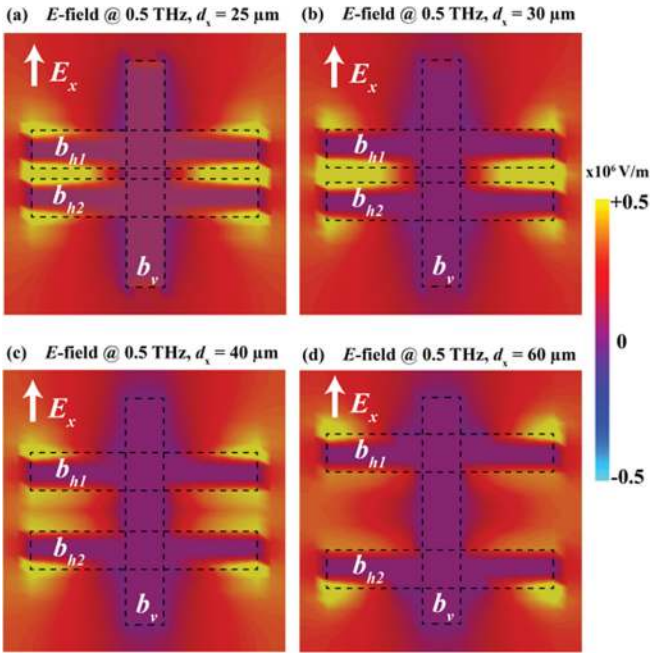

FIG. 4. (a)–(d) Spatial distribution of the resonant electric field E_x in a single unit cell consisting of a radiative atom coupled with a quasi-dark atom with a separation d_x varying from 25 μm to 60 μm calculated at the resonance of the transparency peak (0.5 THz). The gradual decrease in the strength of the fields in the gaps between b_{h1} and b_{h2} signifies the increase in the coupling of the quasi-dark mode to the free space field.

Additional to the broadband EIT effect, it is possible to dynamically modulate the EIT window and therefore to switch between different operation states of the metasurface, from the on-state (EIT mode) to the off-state (dipole mode) using a near infrared pump pulse at room temperature. The active control of the metamaterial resonances has been achieved by integrating the resonator structures with MEMS,[35,36] semiconductors such as GaAs,[37] silicon,[38–41] temperature-driven high-κ dielectrics,[13,42] and recently the perovskites[43,44] that have provided a vital role in achieving the new generation active metadevices. The active metamaterial sample was fabricated on silicon on sapphire (SoS) substrate using two step photolithography processes. As the first step, a 200 nm thick aluminum metal was deposited on a SoS wafer comprising of a 600 nm thick silicon epilayer and a 460 μm thick sapphire substrate, later a positive photoresist was placed in the gaps of the structure, and the reactive ion etching (RIE) process was performed to remove the undesired silicon from the structure. The optical micrograph of the fabricated hybrid metal-semiconductor photoactive metamaterial sample is shown in the inset of Fig. 5(a). The geometrical dimensions are identical to those of Fig. 1(b). The photoactive EIT sample was characterized by using an optical pump-terahertz probe (OPTP) based terahertz time domain spectroscopy system, and the measured data are depicted in Fig. 5(a). An optical pulse with a pulse width of 120 fs and a wavelength of 800 nm is used to photo-excite the silicon patches placed in the gaps between the horizontal bars, and the change in the optical response of the sample was probed by the terahertz pulse. The optical pump and the terahertz probe are illuminated at the normal incidence with an approximate beam diameter of the optical pump and the terahertz probe beam being 10 mm and 4 mm, respectively. The spatial overlap and temporal overlap of the pump-probe beams are accurately matched to achieve the maximum photo-excitation response of the silicon pads. As the pump power is increased from 0 mW to 100 mW (127 μJ cm^{-2}), the EIT window shows a gradual reduction in its amplitude and finally results in a dipolar resonance that completely annihilates the EIT effect in the system, as shown in Fig. 5(a). The active modulation of the EIT window is caused by the photoexcitation of the free carriers in the silicon patches present at the gaps, which gradually weakens the strength of the quasi-dark state in the system. Numerically, we applied a simple conductivity model for both the silicon and the sapphire, considering a constant permittivity of $\varepsilon_{Si} = \varepsilon_{Sap} = 11.7$ and a pump-power-dependent photoconductivity σ_{Si} varying from 0 S/m to 5000 S/m. The conductivity values used in the simulations are the experimentally extracted numbers from the measured photoconductivity spectra of the Si pad with respect to the change in the power of the optical excitation pulse using OPTP measurements. As the conductivity of the Si pads is gradually increased from 0 S/m to 5000 S/m, the transparency window undergoes a strong modulation, as illustrated in Fig. 5(b). Note that the modulation depth depends on the sensitivity of the resonance and the photoconductive response of the deposited silicon patch. The EIT resonance is a result of the interference effect, which would be more sensitive to the external perturbation, and hence, the modulation depth of the device shows an improvement over other dynamic devices.[38–40]

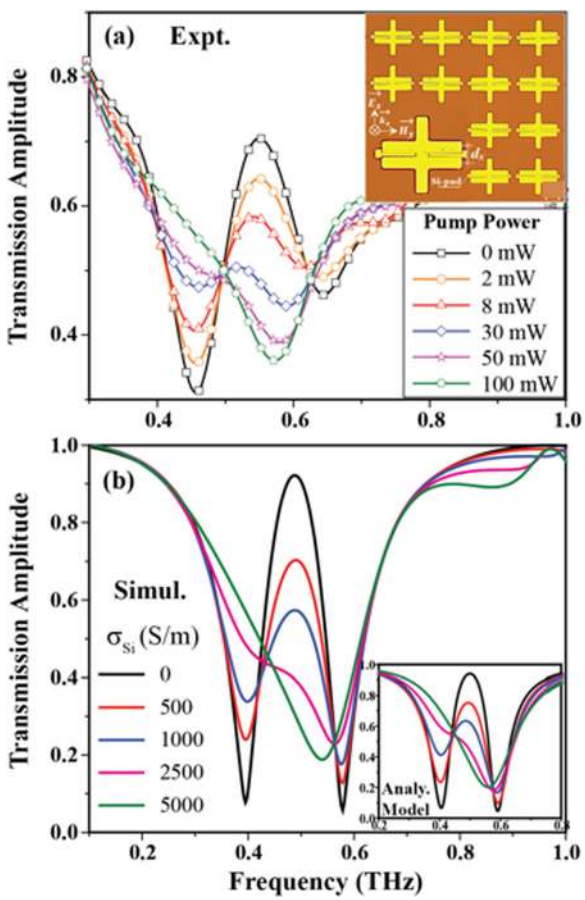

FIG. 5. (a) Transmission spectra showing the active modulation of the EIT window measured using the optical pump-terahertz probe measurements. The inset figure represents the optical micrograph of the fabricated SoS based active EIT metasurface with a separation $d_x = 25\,\mu$m. (b) Evolution of the simulated transmission spectra of the tunable EIT metamaterial with varying conductivities σ_{Si} of the photoconductive silicon pads in the range of 0–5000 S/m. One to one correspondence of the conductivity values used in the simulation to the experimental optical pulse powers is shown by the identical colored plots in Figs. 4(a) and 4(b), respectively. The analytically modeled data are presented in the inset figure (b) that shows good agreement with the simulated curves.

Further, we apply the proposed coupled oscillator model [Eqs. (1)–(3)] to comprehend the changes in the resonance parameters of the quasi-dark resonator structures due to the varying photoconductivity of the silicon pads present in the gaps. The transmission spectra derived from the analytical model are illustrated in the inset of Fig. 5(b), which show very close agreement with the corresponding numerically simulated spectra. The retrieved parameters from the analytically fitted data suggest that the increase in the radiative line widths (loss factors) and the free-space coupling factors of the quasi dark mode result in decreasing amplitude of the EIT window. The coupling constant (Ω) and the resonance frequencies (ω_b and ω_d) for the bright and quasi-dark mode coupling stay the same, whereas the loss factors of the quasi-dark mode vary from $\gamma_d = 0.1\gamma_b$ to $2\gamma_b$ and the free space coupling ratio f_b/f_d decreases from 10 to 2, when the conductivity of the silicon patches in the gaps is changed from 0 S/m to 5000 S/m. Henceforth, by actively modulating the radiative characteristics of the quasi-dark mode in the proposed EIT system, the transparency window can be switched on

and off at a time scale of few milliseconds that is entirely determined by the recombination lifetime of sandwiched silicon.

The potential applications of the proposed EIT metamaterial include biosensing and slow-light devices. Indeed, one can take advantage of the two resonance dips on both sides of the transparency window for dual band sensing applications.[45] Furthermore, the strong dispersion in the vicinity of the EIT window is a key parameter that significantly reduces the group velocity, which renders our structure very attractive for slow light applications.

In summary, we have designed, fabricated, and experimentally characterized a broadband classical analogue of electromagnetically induced transparency (EIT) in the symmetric configuration of the metamaterial structure in the THz regime. Using the silicon pads in the gaps of the horizontal resonators (quasi-dark modes), we demonstrated the active modulation of the EIT effect by actively changing the radiative characteristics of the quasi-dark mode with the illumination of the near infrared optical pulse. The observed broadband and the active modulation results of the EIT effect were modeled using the coupled oscillators, which showed good agreement with the observed results. The compactness of the structure, the simple topology of the resonators, and the ease of engineering the transmission bandwidth are all key parameters that show potential and a wide array of applications in the low cost device based platforms that include biosensors, THz modulators, and slow-light devices.

R. Singh would like to thank his start up (Grant No. M4081282) and Singapore Ministry of Education (MOE) (Grant No. MOE2015-T2-2-103).

[1]N. Liu, T. Weiss, M. Mesch, L. Langguth, U. Eigenthaler, M. Hirscher, C. Sönnichsen, and H. Giessen, Nano Lett. **10**, 1103 (2010).
[2]R. Yahiaoui, A. C. Strikwerda, and P. U. Jepsen, IEEE Sens. J. **16**, 2484 (2016).
[3]J. J. Longdell, E. Fraval, M. J. Sellars, and N. B. Manson, Phys. Rev. Lett. **95**, 063601 (2005).
[4]K. Totsuka, N. Kobayashi, and M. Tomita, Phys. Rev. Lett. **98**, 213904 (2007).
[5]M. F. Yanik, W. Suh, Z. Wang, and S. Fan, Phys. Rev. Lett. **93**, 233903 (2004).
[6]P. Tassin, L. Zhang, T. Koschny, E. N. Economou, and C. M. Soukoulis, Phys. Rev. Lett. **102**, 053901 (2009).
[7]S. E. Harris, J. E. Field, and A. Imamoğlu, Phys. Rev. Lett. **64**, 1107 (1990).
[8]M. Fleischhauer, A. Imamoglu, and J. P. Marangos, Rev. Mod. Phys. **77**, 633 (2005).
[9]J. B. Pendry, Phys. Rev. Lett. **85**, 3966 (2000).
[10]L. Cong, S. Tan, R. Yahiaoui, F. Yan, W. Zhang, and R. Singh, Appl. Phys. Lett. **106**, 031107 (2015).
[11]H. Němec, C. Kadlec, F. Kadlec, P. Kužel, R. Yahiaoui, U.-C. Chung, C. Elissalde, M. Maglione, and P. Mounaix, Appl. Phys. Lett. **100**, 061117 (2012).
[12]D. R. Smith, J. B. Pendry, and M. C. K. Wiltshire, Science **305**, 788 (2004).
[13]H. Němec, P. Kužel, F. Kadlec, C. Kadlec, R. Yahiaoui, and P. Mounaix, Phys. Rev. B: Condens. Matter Mater. Phys. **79**, 241108 (2009).
[14]R. Yahiaoui, H. Němec, P. Kužel, F. Kadlec, C. Kadlec, and P. Mounaix, Opt. Lett. **34**, 3541 (2009).
[15]R. Taubert, M. Hentschel, J. Kästel, and H. Giessen, Nano Lett. **12**, 1367 (2012).
[16]B. Luk'yanchuk, N. I. Zheludev, S. A. Maier, N. J. Halas, P. Nordlander, H. Giessen, and C. T. Chong, Nat. Mater. **9**, 707 (2010).
[17]R. Yahiaoui, K. Hanai, K. Takano, T. Nishida, F. Miyamaru, M. Nakajima, and M. Hangyo, Opt. Lett. **40**, 3197 (2015).
[18]R. Yahiaoui, J. P. Guillet, F. de Miollis, and P. Mounaix, Opt. Lett. **38**, 4988 (2013).
[19]S. Zhang, D. A. Genov, Y. Wang, M. Liu, and X. Zhang, Phys. Rev. Lett. **101**, 047401 (2008).
[20]N. Papasimakis, V. A. Fedotov, and N. I. Zheludev, Phys. Rev. Lett. **101**, 253903 (2008).
[21]R. Singh, C. Rockstuhl, F. Lederer, and W. Zhang, Phys. Rev. B **79**, 085111 (2009).
[22]S.-Y. Chiam, R. Singh, C. Rockstuhl, F. Lederer, W. Zhang, and A. A. Bettiol, Phys. Rev. B **80**, 153103 (2009).
[23]M. Manjappa, S.-Y. Chiam, L. Cong, A. A. Bettiol, W. Zhang, and R. Singh, Appl. Phys. Lett. **106**, 181101 (2015).
[24]M. Manjappa, S. P. Turaga, Y. K. Srivastava, A. A. Bettiol, and R. Singh, Opt. Lett. **42**(11), 2106–2109 (2017).
[25]X. Su, C. Ouyang, N. Xu, S. Tan, J. Gu, Z. Tian, J. Han, F. Yan, and W. Zhang, IEEE Photonics J. **7**, 5900108 (2015).
[26]C. Wu, A. B. Khanikaev, and G. Shvets, Phys. Rev. Lett. **106**, 107403 (2011).
[27]N. Liu, L. Langguth, T. Weiss, J. Kästel, M. Fleischhauer, T. Pfau, and H. Giessen, Nat. Mater. **8**, 758 (2009).
[28]F. Hao, Y. Sonnefraud, P. V. Dorpe, S. A. Maier, N. J. Halas, and P. Nordlander, Nano Lett. **8**, 3983 (2008).
[29]M. Manjappa, Y. K. Srivastava, and R. Singh, Phys. Rev. B **94**, 161103(R) (2016).
[30]X. Jin, Y. Lu, H. Zheng, Y. P. Lee, J. Y. Rhee, and W. H. Jang, Opt. Express **18**, 13396 (2010).
[31]M. Miyata, J. Hirohata, Y. Nagasaki, and J. Takahara, Opt. Express **22**, 11399 (2014).
[32]F.-Y. Meng, Q. Wu, D. Erni, K. Wu, and J.-C. Lee, IEEE Trans. Microwave Theory Tech. **60**, 3013 (2012).
[33]R. Yahiaoui, K. Takano, F. Miyamaru, M. Hangyo, and P. Mounaix, J. Opt. **16**, 094014 (2014).
[34]M. Wan, Y. Song, L. Zhang, and F. Zhou, Opt. Express **23**, 27361 (2015).
[35]H. Tao, A. C. Strikwerda, K. Fan, W. J. Padilla, X. Zhang, and R. D. Averitt, Phys. Rev. Lett. **103**(14), 147401 (2009).
[36]P. Pitchappa, M. Manjappa, C. P. Ho, R. Singh, N. Singh, and C. Lee, Adv. Opt. Mater. **4**(4), 541–547 (2016).
[37]W. J. Padilla, A. J. Taylor, C. Highstrete, M. Lee, and R. D. Averitt, Phys. Rev. Lett. **96**, 107401 (2006).
[38]H.-T. Chen, J. F. O'Hara, A. K. Azad, A. J. Taylor, R. D. Averitt, D. B. Shrekenhamer, and W. J. Padilla, Nat. Photonics **2**, 295 (2008).
[39]J. Gu, R. Singh, X. Liu, X. Zhang, Y. Ma, S. Zhang, S. A. Maier, Z. Tian, A. K. Azad, H.-T. Chen, A. J. Taylor, J. Han, and W. Zhang, Nat. Commun. **3**, 1151 (2012).
[40]S. Zhang, J. Zhou, Y.-S. Park, J. Rho, R. Singh, S. Nam, A. K. Azad, H.-T. Chen, X. Yin, A. J. Taylor, and X. Zhang, Nat. Commun. **3**, 942 (2012).
[41]M. Manjappa, Y. K. Srivastava, L. Cong, I. Al-Naib, and R. Singh, Adv. Mater. **29**, 1603355 (2017).
[42]R. Yahiaoui, H. Němec, P. Kužel, F. Kadlec, C. Kadlec, and P. Mounaix, Appl. Phys. A **103**, 689 (2011).
[43]M. Manjappa, Y. K. Srivastava, A. Solanki, A. Kumar, T. C. Sum, and R. Singh, "Hybrid lead halide perovskites for ultrasensitive photoactive switching in terahertz metamaterial devices," Adv. Mater. (published online 2017).
[44]L. Cong, Y. K. Srivastava, A. Solanki, T. C. Sum, and R. Singh, "Perovskite as a platform for active flexible metaphotonic devices," ACS Photonics (published online 2017).
[45]R. Yahiaoui, S. Tan, L. Cong, R. Singh, F. Yan, and W. Zhang, J. Appl. Phys. **118**, 083103 (2015).